A Novel Compact Wearable Microstrip Patch Antenna for Medical Applications

Sadiq Alhuwaidi
Department of Electrical Engineering
Prince Mohammad Bin Fahd University
Khobar, Saudi Arabia
salhuwaidi@pmu.edu.sa

Tanghid Rashid
Department of Electrical and Computer Engineering
University of Colorado
Colorado Springs, U.S.A.
trashid@uccs.edu

***Abstract*— The modeling, design, fabrication, and analysis of a novel compact microstrip patch antenna in the Industrial, Scientific, and Medical (ISM) frequency range (2.4–2.5 GHz) are presented. Simulations were performed to investigate the performance of the structure using high frequency structure simulator (ANSYS HFSS) and Advanced Design System (ADS). The antenna is printed on Rogers RT/Duroid 5880 substrate and measurements were carried out using a vector network analyzer (VNA) and anechoic chamber. The simulated and measured return loss, gain, bandwidth, radiation pattern, and voltage standing wave ratio (VSWR) were obtained and compared with conventional designs. In addition, the specific absorption rate (SAR) is simulated at different positions to measure the level of electromagnetic waves absorbed by the human head model. The 60 × 60 mm, high gain, low specific absorption rate antenna is expected to contribute to the future development of new detection ways for various diseases.**

Keywords—Advanced Design System (ADS), High-Frequency Structure Simulator (HFSS), Wearable device, Specific absorption rate (SAR), Vector network analyzer (VNA), Medical applications, ISM band.

I. INTRODUCTION

Early detections of deadly diseases and viruses reduce the loss and increase the survival rate of living creatures. Scientists and researchers have drawn a significant effort in increasing public health awareness by developing technological and wearable devices to positively influence the treatment options. In particular, microwave technology, whose frequency is in the range of 0.3–300 GHz, possesses many properties that provide potential for applications including material science, physics, chemistry, astronomy, forensics, electrical engineering, precision engineering, and other research areas in biology and medicine. It has solved challenging problems and will continue to do so in the foreseeable future. The designs in the microwave region have succeeded dramatically in the field of electrical engineering for both practical and motivational value. Plenty of microwave experiments develop an intuitive and physical feeling for microwave phenomena. Exploiting the resolution and penetration features, microwave wearables and imaging systems have attracted interests during the past few decades. They enable the observer to study the dielectric properties in the imaging systems and distinguish between the normal and tumor human tissues. Such study provides early detections of diseases like cancer, which has a high mortality rate. Besides, the detection method is fast, reliable, safe, nondestructive, and nonionizing, that is, it has low photonic energy, has short wavelength, and does not damage DNA.

There has been a great demand for developing a nonionizing, low-cost, reliable, nondestructive technology to screen diagnosis and establish a data extinction between healthy and tumor human tissues. Compared to the traditional existing detection methods such as X-ray mammography, magnetic resonance imaging, and ultrasound, the microwave technology has the potential to provide the solution.

Antenna is considered to be a significant factor in wireless communications and radar systems. The operation of the antenna is based on certain parameters that characterize the electromagnetic theory such as gain, directivity, return loss, radiation pattern, and noise characteristics. A variety of antennas have been developed for various applications, such as wire antennas, aperture antennas, printed antennas, and array antennas. An example of printed antennas is microstrip patch antennas, which can easily be fabricated and printed onto a circuit board with low cost and profile. These reasons favor the use of microstrip patch antennas in a variety of applications, including a phone mobile market and medical applications. Inset feed, quarter wavelength transmission line, coaxial cable, aperture feeds, and coupled feeds are common ways of feeding methods that are considered for microstrip patch antennas. In addition, different patch shapes can be designed with microstrip patch antennas to provide the desired results with respect to a particular property.

Extensive efforts have previously been conducted to model, design, and fabricate wearable antennas for various biomedical applications [1-10]. Each design has trade-offs to achieve the desired specifications. For example, an array antenna enlarges the antenna dimensions but enhances the gain, if matched properly. Another example is designing a compact antenna with limited gain, penetration, resolution, efficiency, or bandwidth.

This research was funded by Prince Mohammad Bin Fahd Center for Futuristic Studies (PMFCFS)

978-1-7281-6535-6/20/$31.00 ©2020 IEEE

This study proposes designing a noninvasive cancer screening and detection microstrip antenna in the frequency range of 2.4–2.5 GHz using ADS and HFSS [11-12]. The proposal suggests using a simulated human head model to find SAR. The antenna is fabricated and tested in the anechoic chamber with the use of the VNA.

II. ANTENNA DESIGN

The antenna is designed on Rogers RT/Duroid 5880 substrate, with a dielectric constant of 2.20, loss tangent of 0.0009, and thickness of 1.524 mm. First, a typical pentagon antenna was designed based on the desired operating frequency. Figure 1 shows the pentagon patch antenna.

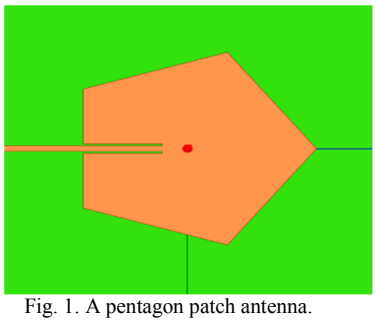

Fig. 1. A pentagon patch antenna.

At first, calculations of the pentagon antenna were obtained based on the typical circular patch [13]. The actual radius of the pentagonal patch can be found as

$$a = \frac{F}{\sqrt{1+\frac{2H}{\pi\varepsilon_r F}\left(\ln\left(\frac{\pi F}{2H}\right)+1.7726\right)}}, \quad (1)$$

where H is the substrate height in cm, ε_r is the dielectric constant, and F is

$$F = \frac{8.791\cdot 10^9}{f_r\sqrt{\varepsilon_r}}, \quad (2)$$

where f_r is the resonant frequency. Equation (1) is the first-order approximation to the solution of

$$a_e = a\sqrt{1+\frac{2H}{\pi a\varepsilon_r}\left(\ln\left(\frac{\pi a}{2H}\right)+1.7726\right)}, \quad (3)$$

where a_e is the effective radius. At resonance, the input impedance of a circular patch is real. Thus, the input resistance for the dominant mode TM_{11} can be expressed as

$$R_{in}(\rho'=\rho_0) = \frac{1}{G_t}\frac{J_1^2(k\rho_0)}{J_1^2(ka_e)}, \quad (4)$$

where J_1 is the Bessel function of first kind of order 1, k is the wavenumber, and G_t is the total conductance due to the radiation, conduction, and dielectric losses determined by

$$G_t = G_{rad} + G_c + G_d, \quad (5)$$

where G_{rad}, G_c, and G_d are the conductance due to radiation, conduction, and dielectric losses, respectively. The resonant input resistance of the circular patch with an inset feed is

$$R_{in}(\rho'=\rho_0) = R_{in}(\rho'=a_e)\frac{J_1^2(k\rho_0)}{J_1^2(ka_e)} \quad (6)$$

$$R_{in}(\rho'=a_e) = \frac{1}{G_t} \quad (7)$$

The directivity of the antenna is

$$D_o = \frac{(k_o a_e)^2}{120 G_{\text{rad}}} \quad (8)$$

The pentagon antenna was reduced in size, which required modifying the geometry to obtain optimum results. Figure 2 shows the modified pentagon antenna design, and Table I summarizes the dimensions.

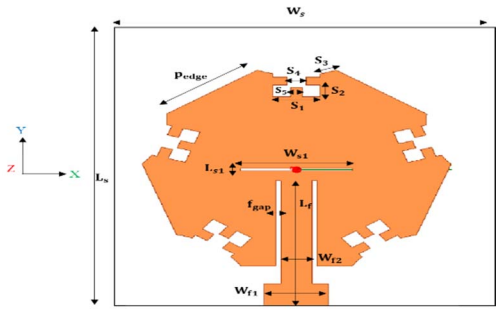

Fig. 2. Pentagon-shaped antenna design.

Table I. Antenna dimensions/parameters.

Parameter	Values	Parameter	Values
ε_r	2.2	t	0.035 mm
h	1.524 mm	$Patch_{radius}$	26.2 mm
$Patch_{edge}$	16.41 mm	W_{f1}	9.398 mm
W_g	60 mm	W_{f2}	4.57 mm
L_g	60 mm	L_f	27.6 mm
W_{s1}	16.48 mm	f_{gap}	0.75 mm
L_{s1}	0.53 mm	S_3	2.43 mm
S_1	7 mm	S_4	2.8 mm
S_2	2.65 mm	S_5	1.7 mm

The antenna consists of pentagon and inset-fed patches. The angles of the pentagon were removed and modified to optimize the antenna parameters. The matching networks are crucial such that the maximum power is delivered and the power loss is minimized when the load is matched to the line [14]. The inset-fed line mechanism was incorporated to properly match the impedance and increase the gain. The overall size of the antenna is 60 × 60 mm. Figure 3 shows the side view of the antenna design.

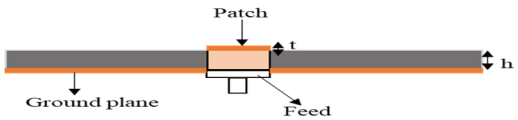

Fig. 3. Side view of antenna.

Figure 4 shows the bottom side of the antenna.

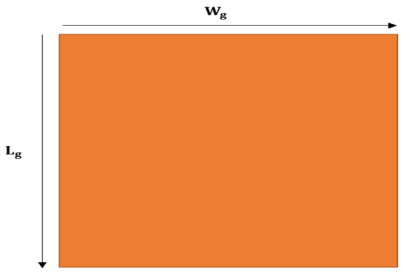

Fig. 4. Bottom view of antenna.

III. SIMULATIONS

This section highlights the performed simulations in HFSS and ADS to characterize the antenna.

A. Antenna Design in HFSS

The antenna was characterized using HFSS. Figure 5 illustrates the gain of the antenna at 2.44 GHz.

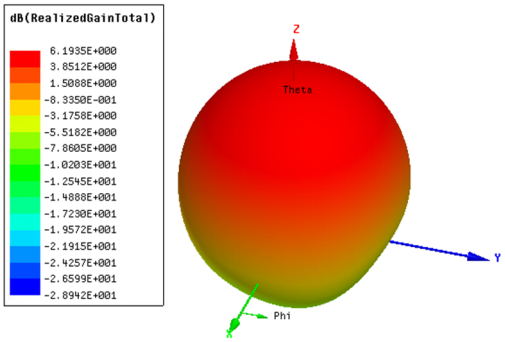

Fig. 5. Gain of antenna at 2.44 GHz.

As shown in Fig. 5, the maximum gain is 6.19 dB. Figure 6 shows the electric field distribution through the antenna at 2.44 GHz.

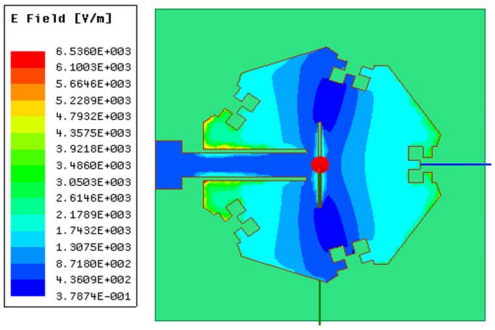

Fig. 6. E-field distribution in antenna using HFSS.

The electric field is focused on the edges close to the feeding path. Figure 7 shows the surface current distributions at 2.44 GHz.

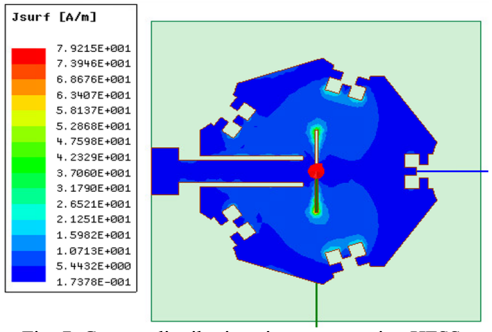

Fig. 7. Current distributions in antenna using HFSS.

As shown in Fig. 7, the current is clustered and focused around the slot in the middle.

B. Antenna Design in ADS

The antenna was characterized using ADS. Figure 8 illustrates the antenna in the layout window of ADS.

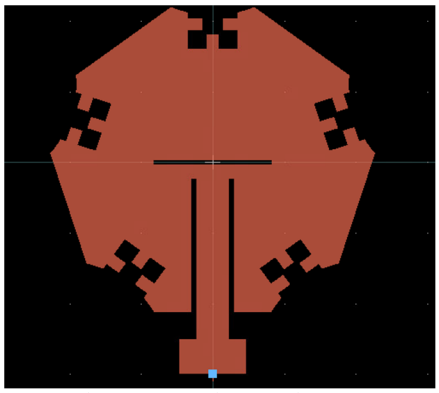

Fig. 8. Layout of antenna in ADS.

C. SAR

The antenna is brought next to a human head model to evaluate the antenna performance on the body through SAR. Such antenna is placed at different locations and positions to determine the SAR value. Figure 9 shows the side view of human head model used to determine the SAR.

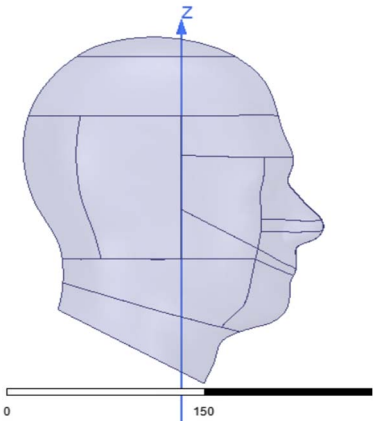

Fig. 9. Side view of a human head model.

Figure 10 shows the top view of the human head model.

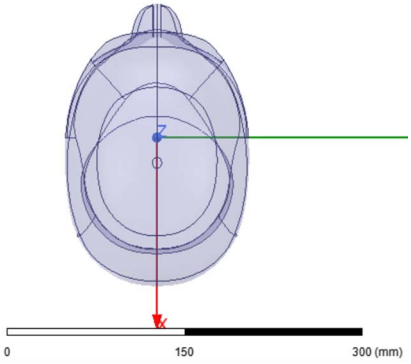

Fig. 10. Side view of a human head model.

The simulated average SAR is compared with the American and European SAR standards, indicating that the results must be below 1.6 W/kg for tissue in 1 g as per American standard and 2 W/kg for tissue in 10 g as per European standard.

IV. FABRICATIONS

The simulation file of the antenna was exported as a Gerber file in order for the ProtoMat machine to recognize the file and import the layout. An SMA connector was soldered in the board. Figure 11 shows the fabricated antenna with a size of 60 × 60 mm.

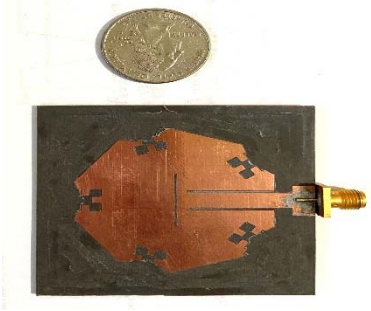

Fig. 11. Fabricated antenna.

The antenna was connected to the VNA through the SMA connector to obtain the frequency response of S_{11} in dB with the desired frequency range. Figure 12 shows the S_{11} measurements setup.

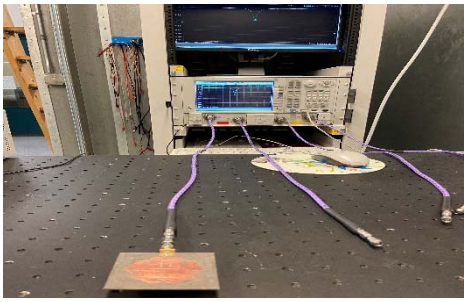

Fig. 12. S_{11} measurements setup of antenna.

The scattering parameter, S_{11}, was obtained from the VNA. Figure 13 shows the simulated and measured return loss measurements of the antenna.

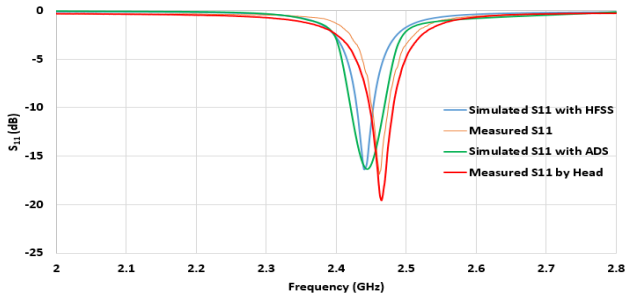

Fig. 13. Simulated and measured return loss of antenna.

As shown in Fig. 13, the blue curve represents the simulated return loss using HFSS. HFSS uses the finite element method volume meshing for arbitrary 3D modeling. Its lowest value is −16.4 dB at 2.44 GHz, and the bandwidth is about 1%. The green curve represents the simulated return loss using ADS. ADS uses momentum (MOM) for planar 3D modeling. Its lowest value is −16.3 dB at 2.44 GHz, and the bandwidth is about 2%. The Paige curve represents the measured return loss. Its lowest value is −16.9 dB at 2.46 GHz, and the bandwidth is about 1%. The red curve represents the measured return loss when brought close to the human head. Its lowest value is −19.6 dB at 2.46 GHz, and the bandwidth is about 1.3%. Such measurements were performed after verifying SAR, discussed in this section. Figure 14 shows the return loss measurement setup of the antenna when brought close to the human head.

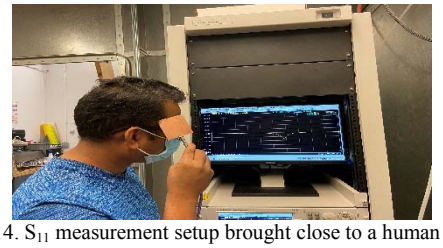

Fig. 14. S_{11} measurement setup brought close to a human head.

The voltage standing wave ratio (VSWR) was investigated to check the efficiency of the antenna and is defined by

$$VSWR = \frac{1+|\Gamma|}{1-|\Gamma|} \quad (1)$$

Figure 15 illustrates the simulated and measured voltage standing wave ratio of the antenna.

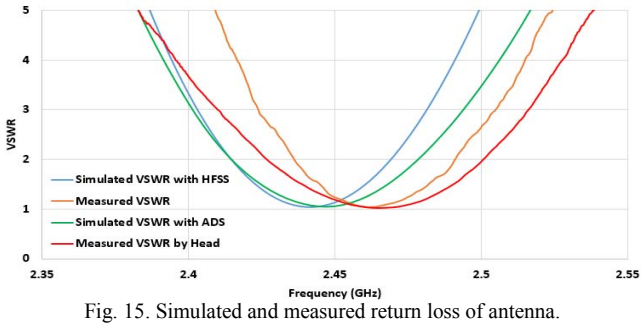

Fig. 15. Simulated and measured return loss of antenna.

As shown in Fig. 15, VSWR is less than two in the operating frequency. Thus, more power is delivered to the antenna at the desired band. In addition, the simulated gain and efficiency of the antenna were investigated. Table II summarizes the simulated gain and efficiency results using HFSS and ADS.

Table II. Simulated gain and efficiency using HFSS and ADS.

Software	Simulations	
	Gain (dB)	*Efficiency (%)*
HFSS	6.19	82.9
ADS	6.71	86.6

The gain values in HFSS and ADS differ by 0.52 dB because the efficiency and directivity were different. In addition, the radiation pattern of the pentagon antenna was simulated using HFSS and measured in anechoic chamber from −180° to 180°. Figure 16 demonstrates the normalized simulated and measured radiation pattern.

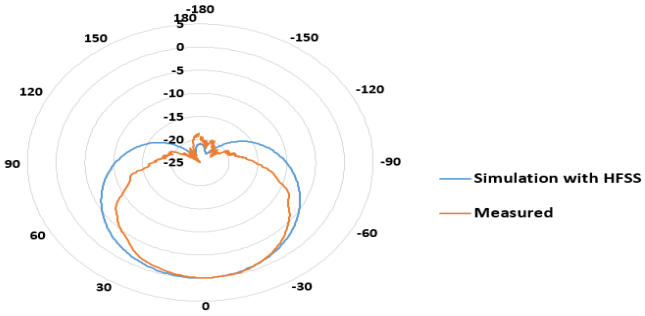

Fig. 16. Simulated and measured normalized radiation pattern of pentagon antenna.

As shown in Fig. 16, close agreements occur between the simulated and measured normalized patterns throughout the 360°. The measurements of such radiation pattern involve using an EMCO 3115 double ridge horn transmitting antenna, input power of 12 dBm, and low noise amplifier supplied at 15 V in the far-field region. The proposed antenna is the receiving antenna. Figure 17 shows the radiation pattern measurements setup.

Fig. 17. Anechoic chamber setup to measure the radiation antenna of pentagon antenna.

The pentagon antenna was placed at two different locations to determine the simulated SAR. For each location, the antenna was positioned at three different distances between the head and antenna. That is, the antenna was placed at 2 mm, 20 mm, and 40 mm near the temple at the top of the head. Figure 18 shows the two different locations of the pentagon antenna used to determine SAR.

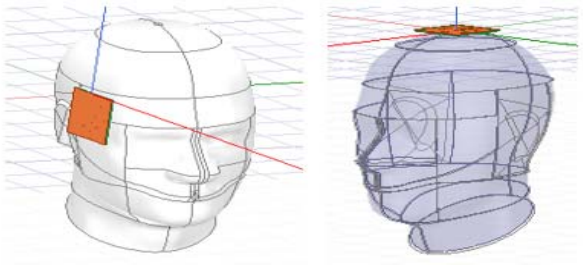

Fig. 18. Pentagon antenna near the temple and at the top of the head to determine SAR.

Figure 19 shows the SAR profile of the pentagon antenna near the temple.

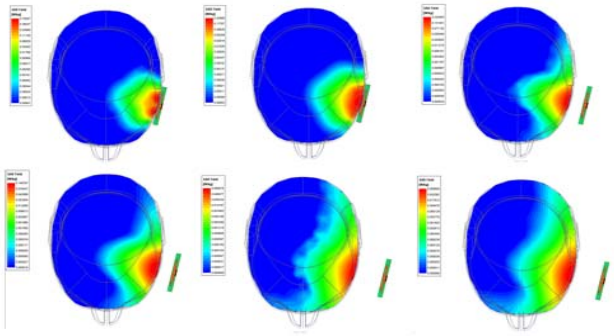

Fig. 19. SAR profile of the pentagon antenna near the temple.

Figure 20 shows the SAR profile of the pentagon antenna at the top of head.

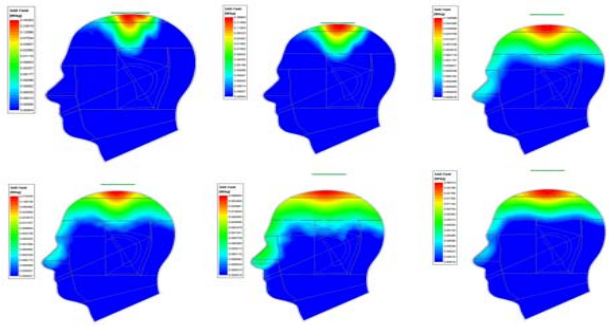

Fig. 20. SAR profile of the pentagon antenna at the top of the head.

Tables III and IV summarize the SAR results near the temple and at the top of head of the pentagon antenna using HFSS.

Table III. SAR of pentagon antenna near the temple.

Input Power (mW)	Head to Antenna Distance (mm)	Average SAR (W/kg) in 1 g Tissue	Average SAR (W/kg) in 10 g Tissue
15.84	2	0.59	0.22
	20	0.23	0.13
	40	0.08	0.05

Table IV. SAR of pentagon antenna at the top of head.

Input Power (mW)	Head to Antenna Distance (mm)	Average SAR (W/kg) in 1 g Tissue	Average SAR (W/kg) in 10 g Tissue
15.84	2	0.69	0.26
	20	0.25	0.13
	40	0.09	0.05

As summarized in Tables III and IV, the maximum simulated SAR values occur when the antenna is closest to the head. Such values are below the SAR values in the American and European standards. The simulated and measured results of the modified pentagon antenna were compared with the existing designs [15-21]. Table V summarizes the comparison of the obtained results with existing designs.

Table V. Comparison of parameters between this paper and other existing designs.

Ref	Frequency (GHz)	Gain (dBi)	Size (mm)	Bandwidth (%)
[15]	2.45/5.8	1.77/3.14	986(area) × 1.58	1.2/2.0
[16]	2.45/5.8	2.5/4	100 × 100 × 3	-/15.4
[17]	2.4	4.12	50 × 50 × 9.5	1.88
[18]	2.45	4.2	3326(area) × 3.7	4.8
[19]	2.45	4.8	45 × 30 × N/A	18
[20]	2.4	5.2	50 × 50 × 5.5	11.3
[21]	1.8/2.45	-	150 × 150 × 2	10.92/5.08
This Paper	2.44	6.71	60 × 60 × N/A	1

V. Conclusion

A wearable pentagon microstrip patch antenna was modeled, designed, and fabricated in the ISM band. It is used as a diagnostic tool in medical applications such as detecting brain cancer and head imaging system. Three separate phases constituted the project. The first phase is the simulations of the modified pentagon microstrip antenna. At first, calculations are managed for the typical design based on the desired specifications. The physical dimensions of the patch, including the matching circuits, are calculated in order to properly choose, simulate, and perform the design. The second phase uses microwave computer-aided design software simulations to solve and implement rigorous field theory solutions. Two simulation tools are used to design the microstrip patch antenna, namely, ADS and ANSYS HFSS. The simulation tool involves the human head model to determine SAR. The third phase is the fabrication of the proposed antenna. This study will provide preliminary results for future developing wearable antenna technologies and will facilitate further developments of new detection ways.

Acknowledgment

The authors thank Prince Mohammad Bin Fahd University (PMU), Prince Mohammad Bin Fahd Center for Futuristic Studies (PMFCFS), and World Futures Studies Federation (WFSF) for their support to complete this research.

References

[1] Bashri, M.S., Arslan, T., Zhou, W., & Haridas, N. (2016). Wearable device for microwave head imaging. *2016 46th European Microwave Conference (EuMC)*, 671-674. DOI:10.1109/EuMC.2016.7824432

[2] Neha and A. Kaur, "Wearable antenna for skin cancer detection," 2016 2nd International Conference on Next Generation Computing Technologies (NGCT), Dehradun, 2016, pp. 197-201. DOI: 10.1109/NGCT.2016.7877414

[3] R. Raihan, M. S. A. Bhuiyan, R. R. Hasan, T. Chowdhury and R. Farhin, "A wearable microstrip patch antenna for detecting brain cancer," 2017 IEEE 2nd International Conference on Signal and Image Processing (ICSIP), Singapore, 2017, pp. 432-436. DOI: 10.1109/SIPROCESS.2017.8124578

[4] F. Wang, T. Arslan and G. Wang, "Breast cancer detection with microwave imaging system using wearable conformal antenna arrays," 2017 IEEE International Conference on Imaging Systems and Techniques (IST), Beijing, 2017, pp. 1-6. DOI: 10.1109/IST.2017.8261547

[5] F. Wang, "Assembly conformal antenna array for wearable microwave breast imaging application," Loughborough Antennas & Propagation Conference (LAPC 2017), Loughborough, 2017, pp. 1-5. DOI: 10.1049/cp.2017.0301

[6] F. Alsharif and C. Kurnaz, "Wearable Microstrip Patch Ultra Wide Band Antenna for Breast Cancer Detection," 2018 41st International Conference on Telecommunications and Signal Processing (TSP), Athens, 2018, pp. 1-5. DOI: 10.1109/TSP.2018.8441335

[7] H. Zhang, A. O. El-Rayis, N. Haridas, N. H. Noordin, A. T. Erdogan and T. Arslan, "A smart antenna array for brain cancer detection," 2011 Loughborough Antennas & Propagation Conference, Loughborough, 2011, pp. 1-4. DOI: 10.1109/LAPC.2011.6114045

[8] H. Bahramiabarghouei, E. Porter, A. Santorelli, B. Gosselin, M. Popović and L. A. Rusch, "Flexible 16 Antenna Array for Microwave Breast Cancer Detection," in IEEE Transactions on Biomedical Engineering, vol. 62, no. 10, pp. 2516-2525, Oct. 2015. DOI: 10.1109/TBME.2015.2434956

[9] E. Porter, H. Bahrami, A. Santorelli, B. Gosselin, L. A. Rusch and M. Popović, "A Wearable Microwave Antenna Array for Time-Domain Breast Tumor Screening," in IEEE Transactions on Medical Imaging, vol. 35, no. 6, pp. 1501-1509, June 2016. DOI: 10.1109/TMI.2016.2518489

[10] F. Wang and T. Arslan, "Inkjet-printed antenna on flexible substrate for wearable microwave imaging applications," 2016 Loughborough Antennas & Propagation Conference (LAPC), Loughborough, 2016, pp. 1-4. DOI: 10.1109/LAPC.2016.7807499

[11] Advanced Design System. Agilent Technologies, Santa Clara, CA, 2009.

[12] ANSYS HFSS, 3D Full-wave Electromagnetic Field Simulation by Ansoft. [Online]. Available: https://www.ansys.com/products/electronics/ansys-hfss

[13] Constantine A. Balanis, *Antenna Theory*, 3rd ed., Wiley, 2005.

[14] D. M. Pozar, *Microwave Engineering*, 4th. ed., John Wiley & Sons, 2012.

[15] X.Q. Zhu,Y. X. Guo, and W. Wu, "A compact dual-band antenna for wireless body-area network applications," *IEEE Antennas Wireless Propag. Lett.*, vol. 15, pp. 98–101, 2016.

[16] S.Yan, P. J. Soh, and G.A. E. Vandenbosch, "Low-profile dual-band textile antenna with artificial magnetic conductor plane," *IEEE Trans. Antennas Propag.*, vol. 62, no. 12, pp. 6487–6490, Dec. 2014.

[17] K. Agarwal, Y. X. Guo, and B. Salam, "Wearable AMC backed nearendfire antenna for on-body communications on latex substrate," *IEEE Trans. Compon., Packag., Manuf. Technol.*, vol. 6, no. 3, pp. 346–358, Mar. 2016.

[18] S. Agneessens, S. Lemey, T. Vervust, and H. Rogier, "Wearable, small, and robust: The circular quarter-mode textile antenna," *IEEE Antennas Wireless Propag. Lett.*, vol. 14, pp. 1482–1485, 2015.

[19] H. R. Raad, A. I. Abbosh, H. M. Al-Rizzo, and D. G. Rucker, "Flexible and compact AMC based antenna for telemedicine applications," *IEEE Trans. Antennas Propag.*, vol. 61, no. 2, pp. 524–531, Feb. 2013.

[20] Z. H. Jiang, Z. Cui, T. W. Yue, Y. Zhu, and D. H. Werner, "Compact, highly efficient, and fully flexible circularly polarized antenna enabled by silver nanowires for wireless body-area networks," *IEEE Trans. Biomed. Circuits Syst.*, vol. 11, no. 4, pp. 920–932, Aug. 2017.

[21] S. Velan *et al.*, "Dual-band EBG integrated monopole antenna deploying fractal geometry for wearable applications," *IEEE Antennas Wireless Propag. Lett.*, vol. 14, pp. 249–252, 2015.